Dynamical Stability Analysis of a Hose to the Sky

Frédérick P. Gosselin[a,*], Michael P. Païdoussis[b]

[a]*Département de Génie Mécanique, École Polytechnique de Montréal, Montréal, Québec, Canada*
[b]*Department of Mechanical Engineering, McGill University, Montréal, Québec, Canada*

Abstract

The Stratospheric Shield was proposed as a geoengineering concept to control the Earth's climate and reverse global warming. This approach seeks to release sulphur dioxide (SO_2) aerosols in the stratosphere to decrease the amount of sunlight that reaches the surface of the Earth. It was proposed that this be done by pumping liquefied SO_2 from the ground to the stratosphere in a 30 kilometre long hose supported by aerostats.

In this paper we evaluate the dynamic stability of a hose to the sky considering distributed supportive aerostats and an atomiser nozzle that forces a radial discharge of the fluid at the free end of the pipe. We modelled the pipe as a taut string conveying fluid using the finite element method.

With a nozzle that discharges the flow straight through, we found that the pipe loses stability by buckling when the tension becomes null at least at one location along its length. This instability can be avoided by having a sufficient minimum tension T_0 throughout the whole length of the pipe. The distribution of aerostats does not influence this instability but it modifies the mode shapes and affects the complex frequencies. The atomiser discharging the flow radially at the tip of the pipe has for effect to remove the possibility of an instability; its use is thus recommended. Moreover, we showed that the Coriolis damping can be significant and that by appropriately selecting the number of aerostats as well as the dimensionless flow velocity, stability can be increased. With this in mind, a functional hose to the sky could be designed to maximise Coriolis damping and thus passively damp the motion of the pipe due to forcing from the wind.

Keywords: Linear stability, fluid-structure interactions, hose to the sky, stratospheric shield

1. Introduction

The dynamics of pipes conveying fluid has been the object of research since at least the late 1930s. Initially, the topic attracted researchers' interest because it displayed interesting dynamical behaviour by means of simple mathematical models, amenable to simple analytical or quasi-analytical solutions and to validations via relatively simple experiments Païdoussis (1993, 1998, 2008).

Most of the seminal research on the fundamentals, conducted in the 1950s and 60s, was curiosity-driven. Applications, making use of the fruits of that research emerged 30, 40 and 50

*Corresponding author.
E-mail address: frederick.gosselin@polymtl.ca

years later, and they continue popping up at an accelerating pace: on ocean mining, drilling for oil and gas, carbon sequestration in the ocean, micro/nano applications (Païdoussis, 2010), and most recently on the "Stratospheric Shield" (Intellectual Ventures, 2009) which is the subject of the present study.

The stratospheric shield which has been the subject of a lot of attention in the popular press (Bradbury, 2008; Levitt and Dubner, 2009) is a geoengineering concept to control the Earth's climate and reverse global warming. This approach seeks to increase the amount of sulphur dioxide (SO_2) aerosols in the stratosphere, so as to decrease the amount of sunlight that reaches the surface of the Earth. It amounts to reproducing the effect of a large volcanic eruption such as that of Mount Pinatubo in the Philippines in 1991. The cooling effect of limiting solar radiation is immediate and not long-lasting, as sulphur dioxide aerosols remain in the stratosphere for only a few years (Robock, 2002). By artificially pumping aerosols in the stratosphere, the blocked sunlight could partially offset the climate warming due to greenhouse gases.

On the downside, geoengineering through the release of SO_2 aerosols could have some serious adverse effects on the the hydrological cycle of the Earth. Potentially, it could lead to widespread drought and reduced freshwater resources (Trenberth and Dai, 2007). Moreover, the concept of humans purposely modifying the climate raises important ethical issues (Crutzen, 2006; Shepherd, 2009). The consequences and implications of geoengineering are not completely understood and require additional research before any implementation should be attempted (Shepherd, 2009). On the other hand, better informed decision will result from further analyses to assess the feasibility of the technology. This is what we pursue here.

Where the fluid-conveying pipe comes into play in the stratospheric shield is that it was suggested as the simplest and most cost-effective way to deliver tons of SO_2 aerosols in the stratosphere (Intellectual Ventures, 2009; Davidson et al., 2012). It is proposed to use a 30 kilometre long hose only a few centimetres in diameter, held up vertically by aerostats (or balloons) to carry 100,000 metric tons of SO_2 up to the stratosphere every year. It is the goal of the present paper to investigate theoretically the dynamic stability of such a slender hose and to see if it would be subject to garden-hose instability (Païdoussis, 1998).

This problem is related to that of tethered aerostat stability.Williamson and Govardhan (1997) and Govardhan and Williamson (1997) showed that a tethered sphere could oscillate significantly when subjected to steady flow due to vortex-induced vibrations. Lambert and Nahon (2003) studied numerically through a lumped-mass approach the nonlinear dynamics of a streamlined aerostat tethered to the ground by one single tether. The aerodynamic forces on this streamlined aerostat were modelled with empirical lift, drag and moment coefficients and with no vortex-shedding forcing considered. The stability analysis showed the system to be stable at all wind speeds. Coulombe-Pontbriand and Nahon (2009) used the approach of Lambert and Nahon (2003) to model a spherical aerostat and added a sinusoidal forcing to account for vortex-shedding excitation. In essence, the design of an aerostat will influence its aerodynamic and inertial properties and if its shape is blunt, vortex-induced vibrations can occur. Because the effect of wind is so dependent on the exact geometry of the aerostat, we leave these effects for later studies.

In the current study, we focus our attention on the effect of the internal flow on the hose system. We investigate the effects on stability of: (i) the see-saw tension along the pipe caused by distributed supportive aerostats, (ii) the point masses associated with the aerostats, and (iii) the atomiser nozzle that forces a radial discharge of the fluid at the free end of the pipe.

Nomenclature

g Gravitational acceleration
L Length of the pipe
ℓ Dimensionless length of the smallest pipe element
M Mass of the fluid per unit length
m Mass of the pipe per unit length
m_n Mass of the n^{th} aerostat
N Number of aerostats
R Density ratio of the fluids inside and outside the aerostat
$T(z)$ Tension along the pipe
T_0 Uniform tension component
t Time
U Flow velocity inside the pipe
$\tilde{u}_{\text{cr}}$ Dimensionless numerical critical flow velocity
u Dimensionless flow velocity
u_{cr} Dimensionless critical flow velocity
V_n Volume of the n^{th} aerostat
W Weight of the pipe
$w(z,t)$ Transverse displacement of the pipe
z Vertical coordinate
z_n Vertical coordinate of the n^{th} aerostat
β Mass ratio
β_n Mass ratio of the n^{th} aerostat
$\Gamma(\xi)$ Dimensionless tension
Γ_0 Dimensionless uniform tension component
δ_{nN} Kronecker delta
ε Discharge parameter ($\varepsilon = 0$, discharges straight through; $\varepsilon = 1$ discharges radially)
η Dimensionless transverse displacement of the pipe
ξ Dimensionless coordinate
ρ_i Density of the gas inside the aerostat
ρ_o Density of air around the aerostat
τ Dimensionless time
ω Complex dimensionless frequency

2. Methodology

We consider a pipe, a few centimetres in diameter and of length L, anchored to the ground and reaching 30 kilometres up to the stratosphere, as depicted in Fig. 1 (a). It is suspended from N equally distributed identical aerostats – or balloons – along its length.

Because the aspect ratio of the pipe is so large, its flexural rigidity EI is very small as compared to the tension $T(x)$ along its length, i.e., $EI/TL^2 \ll 1$. For this reason, we model the pipe as a taut string of negligible flexural rigidity. Moreover, we consider the longitudinal deformation of the pipe to be small, $\epsilon_z = T/AE \ll 1$, which insures that the longitudinal and transverse dynamics are decoupled, as their frequencies are vastly different (Anand, 1969). For a pipe of radius r with a thin shell construction, the relationship for the second moment of area $I = Ar^2/2$ allows rewriting the two previous inequalities as

$$r^2/2L^2 \ll \epsilon_z \ll 1. \tag{1}$$

Because of the very large aspect ratio (L/r), the two inequalities (1) can be respected and the linear equation of the small transverse motion $w(z,t)$, adapted from Païdoussis (1998), may be written as

$$\frac{\partial}{\partial z}\left[\left(MU^2 - T(z)\right)\frac{\partial w}{\partial z}\right] + 2MU\frac{\partial^2 w}{\partial z \partial t} + (M+m)\frac{\partial^2 w}{\partial t^2} + \delta(z - z_n)\frac{m_n}{L}\frac{\partial^2 w}{\partial t^2} = 0, \tag{2}$$

where z is the vertical coordinate, M the mass of the fluid per unit length, U the dimensional flow velocity, m the mass of the pipe per unit length and t is the time. The N supporting aerostats are

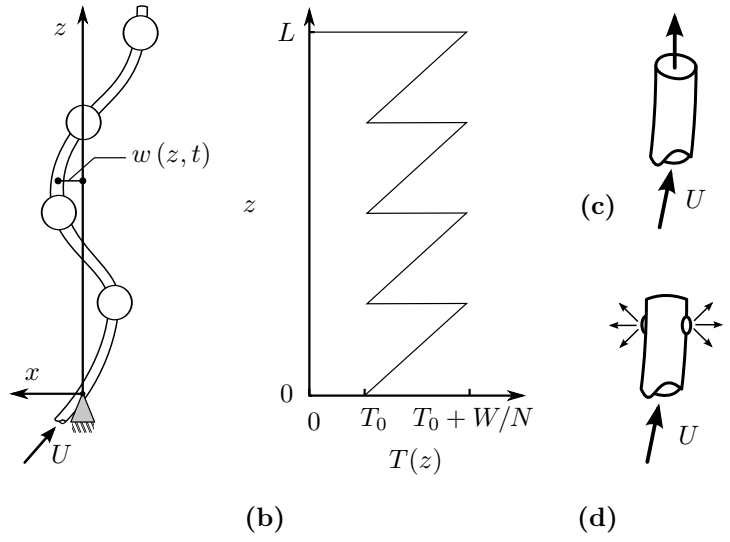

Figure 1: (a) The flexible pipe conveying fluid supported by N aerostats equally distributed along its length, (b) the tension distribution $T(z)$ along the length of the pipe, where $W = (M + m)gL$, (c) the blocked top end of the pipe discharging straight-through flow ($\varepsilon = 0$) and (d) the top end equipped with atomisers discharging the flow radially ($\varepsilon = 1$).

modelled as discrete masses m_n using the Dirac delta function $\delta(z - z_n)$, where $z_n = nL/N$ for $n = 1, 2..N$.

The tension varies along the length of the pipe as depicted in Fig. 1(b). The weight of the pipe is supported by the distributed aerostats, creating this see-saw pattern in the tension. To insure minimal stability, an additional constant tension T_0 is transmitted from the uppermost aerostat to the anchorage on the ground. Moreover, in the case where the pipe is fitted with a stabilising end-piece that atomises the fluid in all radial directions while blocking the straight-through flow-path at the top of the pipe, the momentum of the fluid flow creates a tension MU^2 in the pipe (Rinaldi and Païdoussis, 2010). The total tension in the pipe is thus

$$T(z) = T_0 + (m + M)\, g\, [z \bmod L/N] + \varepsilon MU^2, \tag{3}$$

where $g = 9.81\,\mathrm{m/s^2}$ is the gravitational acceleration which is assumed constant over the length of the pipe, $[z \bmod L/N]$ is the remainder of the division of z by L/N, and ε is the discharge parameter. From Newton's law of universal gravitation, the value of g should be diminished by less than 1% at 30 km above the Earth's surface. Neglecting this variation makes the tension equation slightly more straightforward and should not influence greatly the dynamics.

If the upper tip of the pipe is fitted with atomisers that discharge the conveyed fluid in all directions as in Fig. 1 (d), $\varepsilon = 1$; whereas if the pipe is simply discharging straight through as in Fig. 1 (c), $\varepsilon = 0$.

The pipe is supported by N aerostats equally distributed along its length. For lack of a better design, we assume that all N aerostats are spherical and produce the same lifting force except for the N^{th} aerostat at the top which produces an additional force T_0 in accordance with Eq. (3). The volume of the n^{th} aerostat depends on its altitude (z_n) and is calculated to provide the buoyancy

force equal to $1/N$ the weight of the pipe (plus T_0 for the top aerostat):

$$V_n = \frac{1}{N}\frac{(m+M)\,L}{\rho_o - \rho_i} + \delta_{nN}\frac{T_0}{g\,(\rho_o - \rho_i)}, \tag{4}$$

where $\rho_o(z_n)$ is the density of air around the aerostat, $\rho_i(z_n)$ is the density of the fluid within, and δ_{nN} is the Kronecker delta. The effective mass of the aerostat at altitude z_n is thus

$$m_n = V_n\rho_i + \frac{1}{2}V_n\rho_o. \tag{5}$$

The first term on the r.h.s. of Eq. (5) is the mass of the fluid inside the aerostat, whereas the second term is the added mass of air around the sphere that accelerates with the aerostat. For simplicity, we neglect the mass of the material the balloon is made of. Substituting Eq. (4) into Eq. (5), we can rewrite the mass of an aerostat as

$$m_n = \left[\frac{(m+M)\,L}{N} + \delta_{nN}\frac{T_0}{g}\right]\frac{\frac{1}{2}+R}{1-R}, \tag{6}$$

where $R(z) = \rho_i(z)/\rho_o(z)$ is the density ratio of the fluids inside and outside the aerostat. Assuming that both fluids behave as ideal gases and that both the pressure and the temperature are the same inside and outside the aerostat, R is also the ratio of molar masses. This is convenient because then R does not vary with altitude and so the mass of every aerostat m_n is equal (except for m_N). Because we neglect the weight of the material of the aerostats, the variation of air density with altitude has no effect on the dynamics of the pipe.

We define the following dimensionless parameters:

$$\begin{gathered}\xi = \frac{z}{L},\ \eta = \frac{w}{L},\ \tau = t\sqrt{\frac{g}{L}},\ \beta = \frac{M}{m+M},\ u = \frac{U}{\sqrt{gL}},\\ \Gamma_0 = \frac{T_0}{(M+m)\,gL},\ \Gamma(\xi) = \frac{T(z)}{(M+m)\,gL},\ \beta_n = \frac{m_n}{(m+M)\,L},\end{gathered} \tag{7}$$

to render Eqs. (2), (3) and (6) dimensionless, as follows:

$$\frac{\partial}{\partial\xi}\left[\left(\beta u^2 - \Gamma(\xi)\right)\frac{\partial\eta}{\partial\xi}\right] + 2\beta u\frac{\partial^2\eta}{\partial\xi\partial\tau} + \frac{\partial^2\eta}{\partial\tau^2} + \delta\left(\xi - \xi_n\right)\beta_n\frac{\partial^2\eta}{\partial\tau^2} = 0, \tag{8}$$

$$\Gamma\left(\xi\right) = \Gamma_0 + \left[\xi \bmod 1/N\right] + \varepsilon\beta u^2, \tag{9}$$

$$\beta_n = \left(\frac{1}{N} + \delta_{nN}\Gamma_0\right)\frac{R+\frac{1}{2}}{1-R}. \tag{10}$$

Eqs. (8) and (9) are valid in the domain $0 < \xi < 1$, with boundary conditions $\eta|_{\xi=0} = 0$ and $(\partial\eta/\partial\xi)|_{\xi=1} = 0$.

We adopt a finite-element formulation for this problem (Burnett, 1987). We develop a two-node element $\tilde{\eta}(\xi) = \Phi_i(\xi)\,\eta_i$ based on linear shape functions $\Phi_i(\xi)$ and nodal displacements η_i. We then apply the Galerkin procedure by substituting $\tilde{\eta}(\xi)$ into Eq. (8), multiplying by the shape functions and integrating by parts over the length ℓ of an element. After some manipulation, we obtain the formulation for an element modelling the linear dynamics of a string conveying fluid:

$$\frac{\ell}{3}\begin{bmatrix}1 & \frac{1}{2}\\ \frac{1}{2} & 1\end{bmatrix}\begin{Bmatrix}\ddot{\eta}_a\\ \ddot{\eta}_b\end{Bmatrix} + \beta u\begin{bmatrix}-1 & 1\\ -1 & 1\end{bmatrix}\begin{Bmatrix}\dot{\eta}_a\\ \dot{\eta}_b\end{Bmatrix} + \frac{\overline{\Gamma}}{\ell}\begin{bmatrix}1 & -1\\ -1 & 1\end{bmatrix}\begin{Bmatrix}\eta_a\\ \eta_b\end{Bmatrix} = \begin{Bmatrix}\phi_a\\ -\phi_b\end{Bmatrix}, \tag{11}$$

where $\dot{\{\}} = \partial\{\}/\partial\tau$, $\bar{\Gamma} = \Gamma_0 + \beta u^2(\varepsilon - 1) + \left[\frac{1}{2}(\xi_a + \xi_b) \bmod 1/N\right]$, and ϕ_i represents the external force applied at node i of the element.

The domain is subdivided into N_e elements giving rise to a singular system of $N_e + 1$ second order equations. With the boundary conditions $\eta_0 = 0$ and $\phi_{N_e} = 0$ we obtain a system of N_e equations: $\mathbf{M}_{ij}\ddot{\eta}_i + \mathbf{C}_{ij}\dot{\eta}_i + \mathbf{K}_{ij}\eta_i = 0$. To account for the point masses of the aerostats, the value of β_n is added to the mass matrix at the nodes located at the aerostats. To study the stability of this system, we seek a solution $\eta_i = \hat{\eta}_i \exp \mathrm{i}\omega\tau$, where the real part of the complex frequency ω is the oscillation frequency and the imaginary part corresponds to the damping.

3. Results

The taut string model of the pipe conveying fluid predicts a static instability when the tension becomes null at least at one location along the length of the pipe. In a taut string model, the rigidity is provided by the tension; if the tension becomes null, the pipe buckles. From Eqs (8-9), when the pipe is discharging straight through ($\varepsilon = 0$), this occurs when $\beta u^2 = \Gamma_0$. Thus the critical flow velocity is given by

$$u_{\mathrm{cr}} = \sqrt{\frac{\Gamma_0}{\beta}} = \sqrt{\frac{T_0}{MgL}}, \quad \text{or equivalently} \quad U_{\mathrm{cr}} = \sqrt{\frac{T_0}{L}}. \tag{12}$$

Numerically though, the instability occurs when the tension at the centre of at least one element is zero, i.e., when $\beta u^2 = \Gamma_0 + \ell/2$, where ℓ is the dimensionless length of the element at the location of minimal tension. Thus, the numerical critical flow velocity is

$$\tilde{u}_{\mathrm{cr}} = \sqrt{\frac{\Gamma_0 + \ell/2}{\beta}}. \tag{13}$$

We can see that the size ℓ of the elements must be small in order for $\tilde{u}_{\mathrm{cr}} \to u_{\mathrm{cr}}$. In all the simulations performed here, we use a combination of elements of two different lengths: 10 short elements ($\ell = 4\Gamma_0 \times 10^{-4}$) just above the ground and each aerostat to ensure that $|u_{cr} - \tilde{u}_{\mathrm{cr}}| < 10^{-4}$ and 190 elements for the rest of the pipe length for a total of $N_e = 200$ elements.

To study the behaviour of the pipe numerically, we must provide values for the different parameters. As in the white paper by Intellectual Ventures (2009), we consider a hose 2 cm in diameter made of a composite of mass $0.4\,\mathrm{kg/m^2}$, carrying a mass flow rate of $3.2\,\mathrm{kg/s}$ of liquefied SO_2 with a density of $1460\,\mathrm{kg/m^3}$. Assuming a plug flow, we find a dimensional flow velocity of $U = 7\,\mathrm{m/s}$. From the densities, we find a mass ratio of $\beta = 0.95$. The aerostats considered are filled with helium surrounded by air, thus the ratio of molar masses is $R = 0.138$. The dimensionless mass of the n^{th} aerostat can thus be calculated from Eq. (10), varying with N and Γ_0.

For a constant tension in the pipe, T_0, we consider two scenarios. In the small tension scenario, we impose a tension that ensures a safety factor of 2 on the critical flow velocity in Eq. (12), i.e. we impose $U_{\mathrm{cr}} = 2 \times 7\,\mathrm{m/s}$. This leads to $u_{cr} = 0.0258$ and thus $\Gamma_0 = 6.3 \times 10^{-4}$. In the large tension scenario, we impose a tension everywhere equal or superior to 10% of the weight of the pipe, thus $\Gamma_0 = 0.1$. With this tension, a pipe discharging straight through should become unstable at $u_{\mathrm{cr}} = 0.324$ according to Eq. (12). This corresponds to a dimensional flow velocity of $U_{\mathrm{cr}} = 176\,\mathrm{m/s}$, greatly exceeding the design requirement of $7\,\mathrm{m/s}$. We are justified in studying

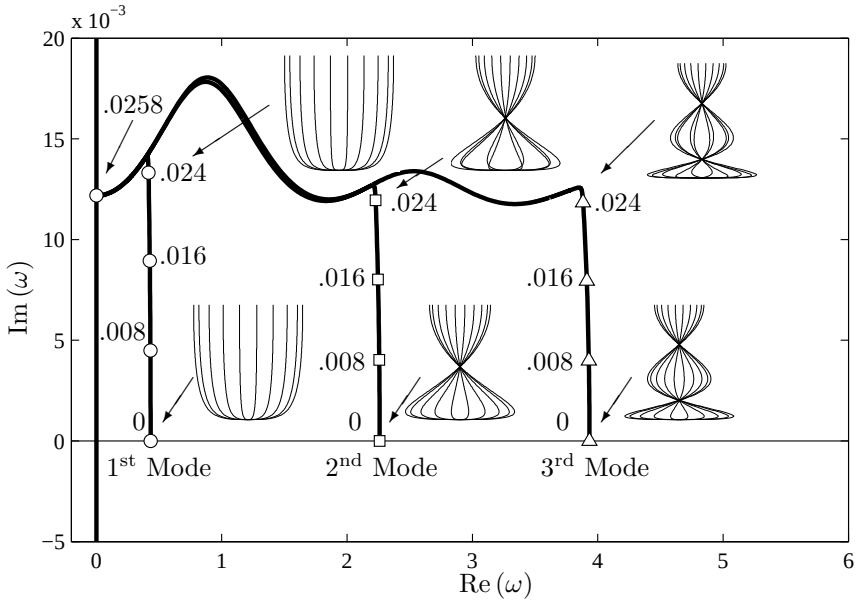

Figure 2: Argand diagram for the first configuration with $\beta = 0.95$, $\Gamma_0 = 0.00063$, $\varepsilon = 0$ and $N = 1$ massless aerostat $\beta_n = 0$. The first three complex frequencies are shown: $\circ$, 1st mode; $\square$, 2nd mode; and $\triangle$, 3rd mode. The corresponding three mode shapes are shown at $u = 0$ and $u = 0.024$.

the second scenario with a tension much greater than that necessary to avoid a static instability, because other considerations such as external forcing by the wind might impose more stringent design criteria on the tensioning.

In order to isolate the influence of each parameter on the dynamics of the pipe, we consider the effects of the tensioning scenario, the mass of the aerostats, the number of aerostats and the discharging nozzle separately. In Figures 2-6, we consider 5 configurations of a pipe supported by : (i) a single massless aerostat with small tension; (ii) a single massless aerostat with a large tension; (iii) a single aerostat with physical mass and large tension; (iv) two aerostats with physical mass and large tension; and (v) two aerostats with physical mass and large tension but discharging radially in opposition to the first four configurations where the pipe discharges straight through.

Considering a pipe supported by $N = 1$ aerostat for the small tension scenario ($\Gamma_0 = 6.3 \times 10^{-4}$), we obtain the Argand diagram shown in Figure 2 for the first three modes. At zero flow, the three frequencies are purely real and thus undamped. As the flow velocity is increased up to $u = 0.024$, the imaginary part of every frequency increases without much effect on the real part. Increasing the flow rate further still, the real part of ω of the first mode becomes zero at $\tilde{u}_{\rm cr} = 0.0258$, whereupon it bifurcates; one branch eventually crosses the origin, so we have the real part equal to zero, while $\mathrm{Im}(\omega) < 0$, which is an indication of a loss of stability by divergence (buckling). The higher modes become unstable for marginally larger flow velocities as the tension at the centre of more elements becomes zero. On the curves of the Argand diagram, the complex frequencies are labelled at regular flow velocity intervals $u = 0$, 0.008, 0.016, 0.024 until instability is reached. No markers appear on the curves between $u = 0.024$ and $\tilde{u}_{\rm cr} = 0.0258$. In that flow velocity range, the real parts of the frequencies suddenly go to zero.

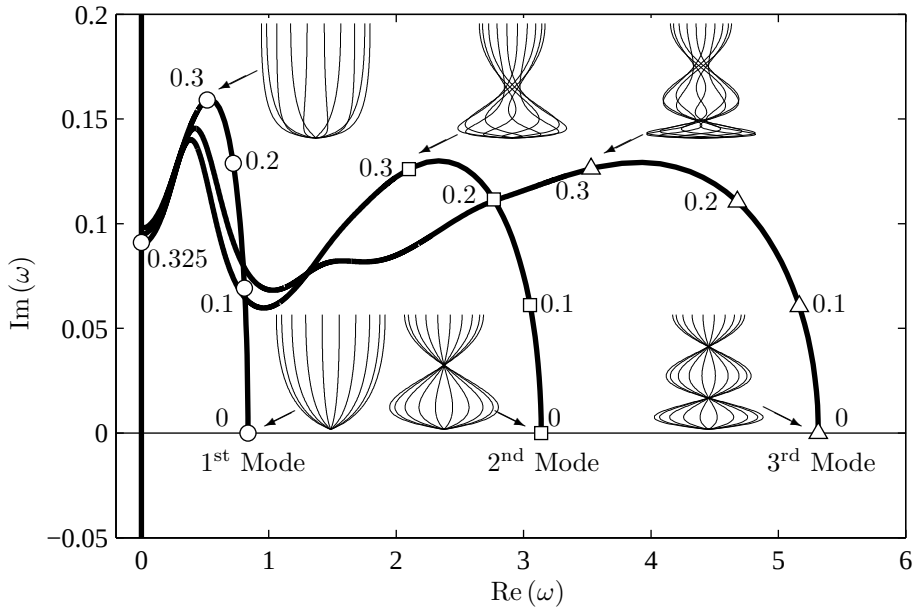

Figure 3: Argand diagram for the second configuration with $\beta = 0.95$, $\Gamma_0 = 0.1$,$N = 1$, $\varepsilon = 0$ and $\beta_n = 0$. The first three complex frequencies are shown: ∘, 1st mode; □, 2nd mode; and △, 3rd mode. The corresponding three mode shapes are shown at $u = 0$ and $u = 0.3$.

The Coriolis term, 2nd on l.h.s. in Eq. (2), is proportional to the flow velocity and is responsible for the increase in damping, hence the term *Coriolis damping* (see Herrmann et al., 1966; Païdoussis, 1998, p.122 and de Langre, 2002, p.97). Since the critical velocity is small for low tension Γ_0, there is little Coriolis damping and the imaginary parts of the frequencies remain small. The real parts of the frequencies are also little affected up to flow velocities close to the critical velocity. Also shown in Fig. 2 are the first three mode shapes at $u = 0$ and $u = 0.024$. The lack of influence of Coriolis damping is obvious in these mode shapes which remain sensibly unaltered up to flow speeds close to the critical flow velocity.

In the next four configurations, we consider the high tension scenario which insures stability up to higher flow speeds and which gives rise to more interesting dynamics as the Coriolis damping becomes more significant.

For the second configuration, considering large tension with one massless aerostat, we obtain the Argand diagram shown in Fig. 3. As in the previous configuration, the frequencies are purely real at zero flow and their imaginary parts become positive as Coriolis damping is generated by the flow. The real part of ω of the first mode becomes zero at $\tilde{u}_{\rm cr} = 0.325$, whereupon it loses stability by buckling.

Because of the higher tension and thus the higher flow velocities considered, the Coriolis damping has more effect on the frequencies and the real parts of the frequencies are significantly altered at flow velocities below the critical velocity. The first three mode shapes at $u = 0$ and $u = 0.3$ are also shown in Fig. 3. With increasing flow speed, the zero-displacement nodes on the 2nd and 3rd modes disappear due to the presence of Coriolis damping. That is because at non-zero flow, the displacement patterns contain both stationary and travelling-wave components. We say that the zero-displacement nodes are replaced by “quasi-nodes”. What is also noticeable is that,

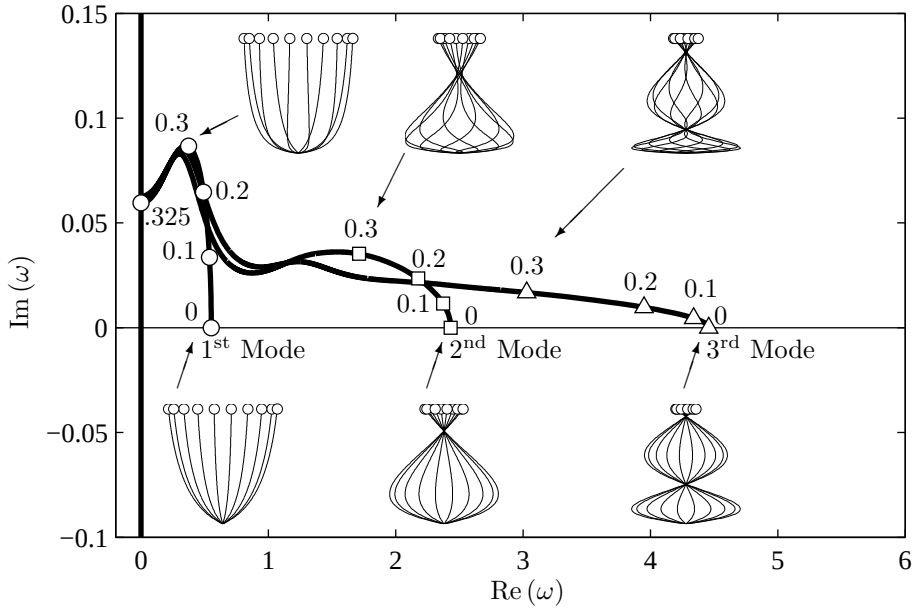

Figure 4: Argand diagram for the third configuration with $\beta = 0.95$, $\Gamma_0 = 0.1$, $N = 2$, $\varepsilon = 0$ and $\beta_n = 0.81$. The first three complex frequencies are shown: ∘, 1st mode; □, 2nd mode; and △, 3rd mode. The corresponding three mode shapes are shown at $u = 0$ and $u = 0.3$.

with higher flow speed, the deformation of the mode shapes is more important at the bottom where the tension is the lowest.

To show the effect of the mass of the aerostat at the top of the pipe in the third configuration, we consider the same parameter values $\beta = 0.95$, $\Gamma_0 = 0.1$ and $N = 1$ as previously, but with a non-negligible aerostat mass $\beta_n = 0.81$. The Argand diagram of the first three frequencies is shown in Fig. 4. The effect of adding mass to the system is to diminish both the real and imaginary parts of all three frequencies. The end-mass thus significantly lowers the effective damping as would be expected when adding mass to a simple mass-spring-dashpot system.

The mode shapes of the first three modes are shown in Fig. 4 at $u = 0$ and $u = 0.3$ with the end-mass depicted as a circle. Comparing with Fig. 3, the end-mass tends to reduce the movement of the tip of the pipe and prolongs the velocity range for the occurrence of nodes. Whereas the nodes in modes 2 and 3 in Fig. 3 clearly become quasi-nodes at $u = 0.3$, the effect is less noticeable in Fig. 4. This is possibly due to the lower damping of these modes.

Subsequently, we study the effect of supporting the hose with two aerostats ($N = 2$) in the fourth configuration. The total mass of the aerostats is the same as in the third configuration but is here split into two, $\beta_1 = 0.37$ and $\beta_2 = 0.44$, and the tension in the pipe has a see-saw pattern. The Argand diagram is shown in Fig. 5, along with the mode shapes. With the same total mass, the first three real frequencies of the system here are lower than for a single larger aerostat (Fig. 4), but the complex part is larger for all flow speeds below $u = 0.3$. The see-saw pattern in the tension function of Eq. (9) due to multiple supporting aerostats significantly affects the appearance of the mode shapes.

The addition of point masses to the system, whether one (Fig. 4), two (Fig. 5) or many more (not shown), does not influence the occurrence of instability. The divergence (buckling)

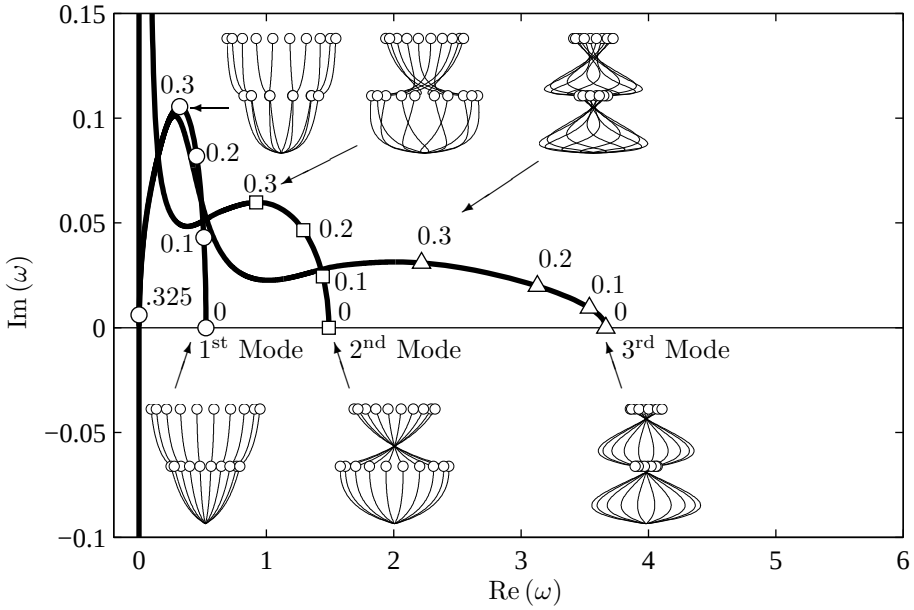

Figure 5: Argand diagram for the fourth configuration with $\beta = 0.95$, $\Gamma_0 = 0.1$, $N = 2$, $\varepsilon = 0$ and $\beta_n = 0.37 + 0.07\delta_{nN}$. The first three complex frequencies are shown: $\circ$, 1st mode; $\square$, 2nd mode; and $\triangle$, 3rd mode. The corresponding three mode shapes are shown at $u = 0$ and $u = 0.3$.

instability is a static loss-of-stiffness instability and is not influenced by the addition of mass. The tension in the pipe becomes zero at $u_{\text{cr}} = 0.324$, no matter how many point-masses are added. However, the loci of the complex frequencies in the Argand diagrams is significantly affected.

Lastly, we study the effect of the atomiser at the end of the pipe in the fifth configuration. Instead of discharging straight through, the pipe now discharges radially. This has for effect the cancellation of the compressive force the fluid flow exerts on the pipe (Eqs. 8 and 9). The Argand diagram for the system with $\varepsilon = 1$ is shown in Fig. 6. The diagram is dramatically different from that of Fig. 5. Notice that the markers in Fig. 6 indicate fluid velocities much higher than in the previous figures (Figs. 2-5). The pipe discharging radially does not have a critical velocity. It does not buckle. However, its modes tend towards null complex frequencies at large flow speeds. The first three mode shapes at $u = 1.0$ are shown on top of Fig. 6. They are not shown at $u = 0$ as they are identical to those of Fig. 5.

The addition of a radial atomiser to discharge the flow radially removes the instability. Atomisers are thus desirable in the design of a SO_2 hose to the sky. However, even if instability is no longer of concern, the dynamic stability analysis of the problem can still bring valuable information for the design of a hose to the sky. For example, the imaginary part of the frequency (or the damping rate) of the first five modes are shown in Fig. 7 versus the number of aerostats at $u = 0.1$ in (a) and at $u = 1.0$ in (b). What can generally be observed is that the damping in a given mode increases rapidly with the number of aerostats N when the latter becomes larger than the number of the mode in question. Also, whereas at low flow speeds (Fig. 7 =(a)) the damping of the first five modes increases monotonically for $N \geq 5$, at higher flow speeds (Fig. 7(b)) the damping decreases with N for large values of N.

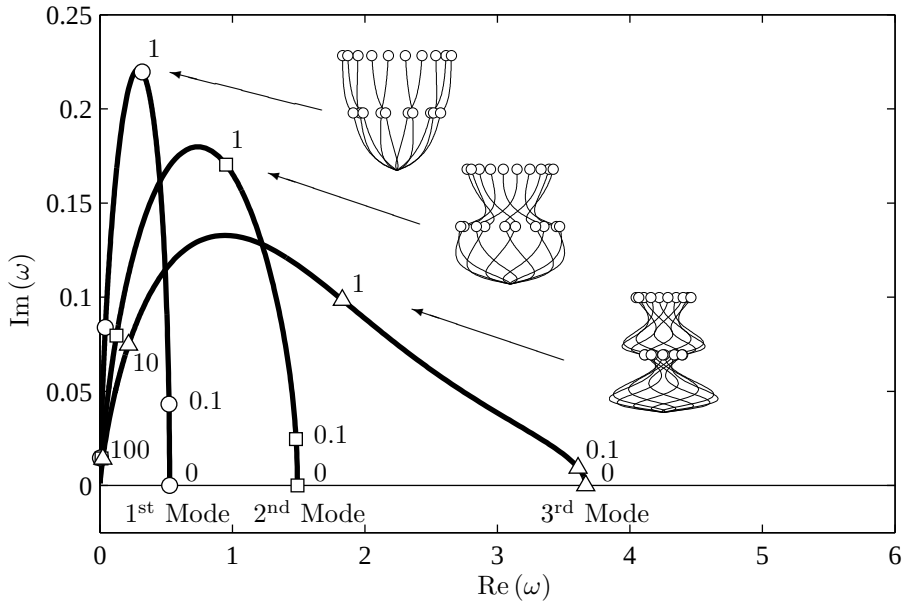

Figure 6: Argand diagram for the fifth configuration, the pipe discharging radially with $\beta = 0.95$, $\Gamma_0 = 0.1$, $N = 2$, $\varepsilon = 1$ and $\beta_n = 0.37 + 0.07\delta_{nN}$. The first three complex frequencies are shown: $\circ$, 1st mode; $\square$, 2nd mode; and $\triangle$, 3rd mode. The corresponding three mode shapes are shown at $u = 1$.

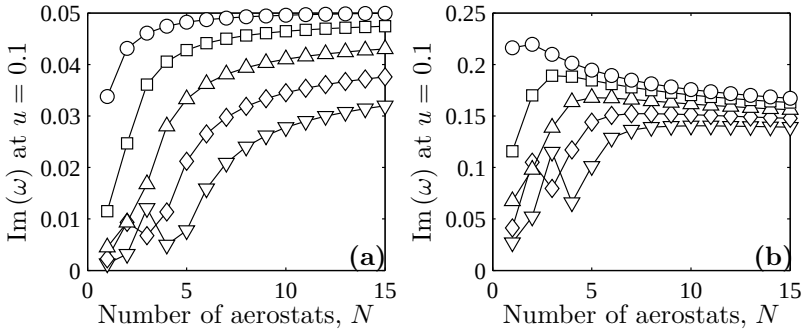

Figure 7: Damping of the vibration modes of the pipe discharging radially ($\varepsilon = 1$) with $\beta = 0.95$, $\Gamma_0 = 0.1$ and $N = 2$ aerostats of mass $\beta_n = 0.37 + 0.07\delta_{nN}$ at flow velocities (a) $u = 0.1$; and (b) $u = 1.0$. The imaginary part of the first fives modes is shown: mode 1 ($\circ$); mode 2 ($\square$); mode 3 ($\triangle$); mode 4 ($\Diamond$); mode 5 ($\triangledown$).

4. Conclusion

The design, construction, deployment and operation of a hose pumping sulphur dioxide to the stratosphere represent tremendous engineering challenges. These come in addition to the simulation and measurement work that must be done to predict and assess the effect of geoengineering on Earth's climate. Here we covered only a very small part of this challenge, by evaluating the dynamic stability of a hose to the sky considering distributed supportive aerostats and the atomiser nozzle that forces a radial discharge of the fluid at the free end of the pipe. We modelled the pipe as a taut string conveying fluid using the finite element method.

With a nozzle that discharges the flow straight through, we found that the pipe loses stability by buckling when the tension becomes null at least at one location along its length. This instability can be avoided by having a sufficient minimum tension T_0 throughout the whole length of the pipe. The distribution of aerostats does not influence this instability but it modifies the mode shapes and affects the complex frequencies. However, if the atomiser discharges the flow radially at the tip of the pipe, the resulting dynamics is radically altered: the instability is totally eliminated. Thus the use of such atomisers is strongly recommended. Moreover, we showed that the Coriolis damping can be significant and that by appropriately selecting the number of aerostats as well as the dimensionless flow velocity it can be increased. With this in mind, a functional hose to the sky could be designed to maximise Coriolis damping and thus passively damp the motion of the pipe. This work may be said to have served to give support to the notion that "the hose to the sky" is a technically feasible way to control the Earth's climate.

The present study is concerned with the effect of internal flow on the dynamic stability of the hose system, but external air flow on the aerostats should also be of significant design concern. The large static wind forces, buffeting and vortex-induced vibrations (Païdoussis et al., 2010) will have important effects on the motion of the aerostats and thus in the stresses experienced by the tether/hose. These phenomena warrant further study, considering both the internal and external flows to account for both the excitation on the pipe and the damping due to internal flow. This could be done by combining the approaches of Govardhan and Williamson (1997), Coulombe-Pontbriand and Nahon (2009) and that of the present study.

Acknowledgements

The authors would like to acknowledge the insightful comments made by anonymous reviewers who helped improve this manuscript, and the funding from the Fonds de Recherche du Québec - Nature et Technologies (FRQNT) and the Natural Sciences and Engineering Research Council of Canada (NSERC).

References

Anand, G., 1969. Large-amplitude damped free vibration of a stretched string. The Journal of the Acoustical Society of America 45 (5), 1089–1096.

Bradbury, D., 2008. Can ecohackers save the planet? The Guardian Weekly, Issue 06/06/2008.

Burnett, D. S., 1987. Finite Element Analysis: From Concepts to Applications. Reading, Massachusetts: Addison-Wesley Pub. Co.

Coulombe-Pontbriand, P., Nahon, M., 2009. Experimental testing and modeling of a tethered spherical aerostat in an outdoor environment. Journal of Wind Engineering and Industrial Aerodynamics 97 (5-6), 208–218.

Crutzen, P., 2006. Albedo enhancement by stratospheric sulfur injections: A contribution to resolve a policy dilemma? Climatic Change 77 (3), 211–220.

Davidson, P., Hunt, H. E. M., Burgoyne, C. J., 2012. Atmospheric delivery system. Patent US 2012/0241554 A1.

de Langre, E., 2002. Fluides et solides. Palaiseau, France: Editions de l'Ecole Polytechnique.
Govardhan, R., Williamson, C., 1997. Vortex-induced motions of a tethered sphere. Journal of Wind Engineering and Industrial Aerodynamics 69 - 71 (0), 375 – 385, Proceedings of the 3rd International Colloquium on Bluff Body Aerodynamics and Applications.
Herrmann, G., Nemat-Nasser, S., Prasad, S. N., 1966. Destabilizing effect of velocity-dependent forces in nonconservative continuous systems. AIAA Journal 4 (7), 1276–1280.
Intellectual Ventures, 2009. The Stratospheric Shield. http://intellectualventureslab.com/wp-content/uploads/2009/10/Stratoshield-white-paper-300dpi.pdf.
Lambert, C., Nahon, M., 2003. Stability analysis of a tethered aerostat. Journal of Aircraft 40 (4), 705–715.
Levitt, S. D., Dubner, S. J., 2009. Super Freakonomics: Global Cooling, Patriotic Prostitutes, and Why Suicide Bombers Should Buy Life Insurance. New York: William Morrow.
Païdoussis, M. P., 1993. Calvin Rice lecture: Some curiosity-driven research in fluid structure interactions and its current applications. ASME Journal of Pressure Vessel Technology 115, 2–14.
Païdoussis, M. P., 1998. Fluid-Structure Interactions: Slender Structures and Axial Flow. London: Academic Press.
Païdoussis, M. P., 2008. The canonical problem of the fluid-conveying pipe and radiation of the knowledge gained to other dynamics problems across applied mechanics. Journal of Sound and Vibration 310 (3), 462–492.
Païdoussis, M. P., 2010. The dynamics of cylindrical conduits containing flowing fluid. 10th Int'l Conference on Computational Structures Technology and 7th Int'l Conference on Engineering Computational Technology, Valencia, Spain; In: Computational Technology Reviews, Vol. 1 (eds B.H.V. Topping, J.M. Adam, F.J. Pallarès, R. Bru & M.L. Romero). Stirlingshire, Scotland: Saxe-Coburg Publications,.
Païdoussis, M. P., Price, S. J., de Langre, E., 2010. Fluid-Structure Interactions: Cross-Flow-Induced Instabilities. Cambridge University Press.
Rinaldi, S., Païdoussis, M., 2010. Dynamics of a cantilevered pipe discharging fluid, fitted with a stabilizing end-piece. Journal of Fluids and Structures 26 (3), 517–525.
Robock, A., Feb. 2002. The climatic aftermath. Science 295 (5558), 1242–1244.
Shepherd, J., 2009. Geoengineering the climate: science, governance and uncertainty. The Royal Society of London.
Trenberth, K. E., Dai, A., 2007. Effects of mount pinatubo volcanic eruption on the hydrological cycle as an analog of geoengineering. Geophysical Research Letters 34 (15), L15702.
Williamson, C., Govardhan, R., 1997. Dynamics and forcing of a tethered sphere in a fluid flow. Journal of Fluids and Structures 11 (3), 293 – 305.